Spectrochimica Acta Part A: Molecular and Biomolecular Spectroscopy 223 (2019) 117296

Contents lists available at ScienceDirect

Spectrochimica Acta Part A: Molecular and Biomolecular Spectroscopy

journal homepage: www.elsevier.com/locate/saa

Theoretical study and experimental validation on the optical emission processes in "free" and "locked" pyrazine derivatives

Tian Zhang [a,*], Fanze Meng [a], Lili Lin [b], Juanjuan Luo [c], Haozhong Wu [c], Xiaojuan Song [a], Chuan-Zeng Wang [a], Hongtao Lin [a], Zhiming Wang [c,*], Shuping Zhuo [a,*]

[a] School of Chemistry and Chemical Engineering, Shandong University of Technology, Zibo 255049, PR China
[b] Shandong Province Key Laboratory of Medical Physics and Image Processing Technology, School of Physics and Electronics, Shandong Normal University, Jinan 250014, PR China
[c] State Key Laboratory of Luminescent Materials and Devices, Center for Aggregation-Induced Emission, Guangzhou International Campus, South China University of Technology, Guangzhou 510640, PR China

ARTICLE INFO

Article history:
Received 2 May 2019
Received in revised form 15 June 2019
Accepted 18 June 2019
Available online 19 June 2019

Keywords:
Pyrazine derivatives
Excited-state properties
Vibrational relaxation
Aggregation-induced emission

ABSTRACT

The excited-state properties of the "free" and "locked" pyrazine derivatives are investigated in solution. DCFP with "free" phenyls is theoretically calculated to be non-emissive due to the non-radiative energy dissipation through strong Duschinsky rotation effect, in agreement with the available experimental result. Surprisingly, DCBP with "bi-locked" phenyls is also calculated to be nonluminous. The emission of DCAP with "conjoined" architecture is predicted to be weaker than DCPP with "single-locked" phenyls, quite contrary to our intuition but further validated by the experimental measurement. The construction of four-, five- and six-membered ring respectively in DCBP, DCAP and DCPP is found to be the major structural origin for the descending relaxation energy in these "locked" systems, thus giving rise to the ascending luminescence order. Our work not only provides strategy for the molecular design of efficient organic light-emitting materials, but also offers valuable insight into the aggregation-induced emission phenomena.

© 2019 Elsevier B.V. All rights reserved.

1. Introduction

Pyrazine derivatives have found applications in organic light-emitting diodes [1,2], light-harvesting platforms [3] and stimuli-responsive materials [4]. The easy preparation and facile modification have turned them into the popular heterocycle-based cores with aggregation-induced emission (AIE) character. AIE-active fluorophores show weak or none emission in solution but strong light in solid state [5]. The electron-deficient feature of the pyrazine ring could serve as a functionalized moiety to achieve structure-dependent emission [6,7]. AIE-active 2,3-dicyano-5,6-diphenylpyrazine with "free" phenyls (DCFP) is non-emissive in tetrahydrofuran (THF) with the fluorescence quantum yield (Φ_f) as low as 0.015%, but non-AIE 2,3-dicyanopyrazino phenanthrene (DCPP) is intensely emissive [8]. The AIE mechanism has been theoretically rationalized by Deng and Wu et al. by conducting comparative studies on DCFP and DCPP, in both gas and solid state [9,10]. The difference in molecular structure between DCFP and DCPP is that DCPP was constructed by linking two phenyls of DCFP through a single covalent bond. Inspired by the conception of locking the phenyl rotors to induce efficient emission in solution, we designed cyclobuta [*def*]triphenylene-2,3-dicarbonitrile (DCBP) and acenaphtho[1,2-*b*]pyrazine-8,9-dicarbonitrile (DCAP). DCBP is figured out by tethering two phenyls in DCFP with two covalent bonds, while DCAP is produced by combination of the two phenyls into the acenaphthylene-based structure. It is primarily the aim of this work to investigate the excited-state properties of these "free" and "locked" pyrazine derivatives and explore the relationship between the locked structures and their respective optical emission properties.

Herein, we performed computational studies on the optical emission processes of DCFP, DCBP, DCAP and DCPP (Fig. 1) in solution. The multi-mode coupled thermal vibrational correlation function (TVCF) formalism was employed to calculate the non-radiative decay rate constants. Experimental validation was also conducted to confirm the theoretical prediction. Our study gains deeper insights into the effect of covalent linkage on the emission quantum efficiency of the pyrazine derivatives.

2. Theoretical and experimental methods

2.1. Ab initio calculations

Geometric and electronic structures were investigated by employing the density functional theory (DFT) at the B3LYP/6-31G(d) level [11,12], which has been shown successful in dealing with the excited-state decay processes of DCFP and DCPP in both gas and cluster phases.

* Corresponding authors.
E-mail addresses: tzhang@sdut.edu.cn (T. Zhang), wangzhiming@scut.edu.cn (Z. Wang), zhuosp_academic@yahoo.com (S. Zhuo).

https://doi.org/10.1016/j.saa.2019.117296
1386-1425/© 2019 Elsevier B.V. All rights reserved.

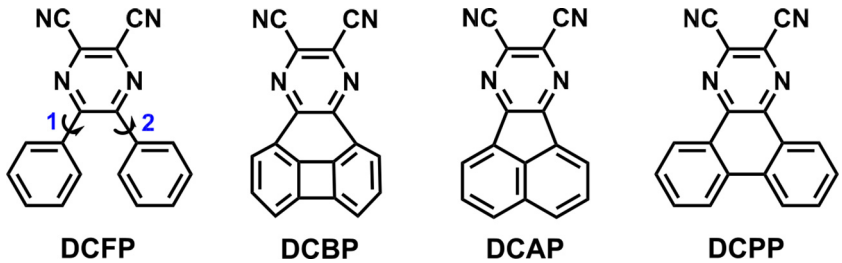

Fig. 1. Molecular structures of DCFP, DCBP, DCAP and DCPP.

Time-dependent DFT (TD-DFT) was applied to optimize the first singlet excited state. The THF solvent environment was mimicked through the polarizable continuum model (PCM) implemented in the Gaussian 16 package [13]. The equilibrium solvation method was applied in both geometry optimizations and frequency calculations, and the non-equilibrium solvation one was used to compute the vertical transition properties [14]. The light-emitting efficiency Φ_f is determined by the competition between the radiative decay rate (k_r) and non-radiative decay rate (k_{nr}). k_{nr} includes the internal conversion rate (k_{ic}) and the intersystem crossing rate (k_{isc}). We ignore k_{isc} because the spin-orbit coupling (SOC) constants between the S_1 and T_1 states of the investigated systems are negligible (<0.1 cm^{-1}), as calculated in the BDF program [15] at their S_1-optimized geometries (Table S1).

k_r can be evaluated through the Einstein spontaneous emission relationship:

$$k_r = \frac{f\Delta E_{vert}^2}{1.499\ \ s \cdot cm^{-2}} \tag{1}$$

where f is the dimensionless oscillator strength of the excited state, ΔE_{vert} is the vertical excitation energy from S_1 to S_0 with the dimension of cm^{-1}.

Based on the perturbation theory and Fermi Golden rule, the analytical formalism of k_{ic} can be expressed as:

$$k_{ic} = \sum_{kl} \frac{1}{\hbar^2} R_{kl} \int_{-\infty}^{\infty} \left[e^{i\omega_{if}t} Z_i^{-1} \rho_{ic,kl}(t,T) \right] dt \tag{2}$$

More details of the correlation function part $\rho_{ic,\ kl}(t,T)$ can be found in Shuai's studies [16,17]. The first-order perturbation theory was applied to compute the nonadiabatic coupling matrix elements R_{kl} following Lin [18]. k_{ic} was calculated by solving the above equation in the MOMAP program [19]. The Gauss broadening width (FWHM) of 17.68 cm^{-1} is adopted in the k_{ic} calculations following Niu [17], to ensure united treatment and convergence of the correlation function. The differences between the potential energy surface (PES) in S_0 and S_1 states are considered by the relationship of the normal-mode coordinates $Q_e = MQ_g + D_e$. M is the Duschinsky rotation matrix (DRM) and D_e is the displacement vector connecting the minima of the S_0 and S_1 parabolas. Normal-mode analyses were also done in the EVC module of the MOMAP program.

2.2. Materials and instruments

All chemicals and reagents were purchased from commercial sources, and used as received without further purification. DCAP and DCPP were prepared according to published procedures [8,20]. ^{1}H NMR spectrum was measured on a VNMRS 500 spectrometer. High resolution mass spectrum (HRMS) was recorded on a GCT premier CAB048 mass spectrometer operating in MALDI-TOF mode. Absorption and photoluminescence (PL) spectra were measured on the Ocean Optics QE65Pro spectrometer. Φ_f was determined by using a Hamamatsu absolute PL quantum yield spectrometer C11347 Quantaurus QY.

3. Results and discussion

3.1. Electronic structures

As shown in the previous studies [9,10], the torsional motions of phenyl rings play important roles in the optical properties of these pyrazine derivatives. Therefore, we presented the representative dihedral angles (Fig. 1) in Table 1, with the geometric parameters at the S_0/S_1 minimum and their modifications. It can be seen that the phenyl rings exhibit remarkable changes of ~15° in DCFP and ~4° in DCBP upon transition, but show almost none variations in DCAP and DCPP. In addition, both DCFP and DCBP possess twisted structures with apparent dihedral angles at the S_0/S_1 minimum, while DCAP and DCPP maintain planar skeletons.

Calculated transition properties from S_1 to S_0 are listed in Table 2. The calculated vertical emission energies well reproduce the experimental peak values with the largest deviation of 0.25 eV. Compared to DCFP, the predicted emission maxima of DCBP and DCPP are remarkably red-shifted, whereas that of DCAP exhibits a slight blue-shift. Both the electric transition dipole moments μ and oscillator strengths f of the three "locked" pyrazine derivatives are much smaller than the "free" DCFP. Based on the natural transition orbital (NTO) analyses [21] for the S_1 states, the transition from the highest occupied NTO (HONTO) to the lowest unoccupied NTO (LUNTO) becomes dominant (>99%) in these systems. As shown in Fig. 2a, the HONTOs and LUNTOs demonstrate π and π* character, respectively. The S_1 states of DCFP and DCAP show local excitation (LE) feature, with the electron density almost distributed on the whole molecular skeleton. Conversely, a hybridized local and charge-transfer (HLCT) property was found for DCBP and DCPP, with LE on the locked two phenyls and CT from the locked part to the cyano-substituted pyrazine ring. The CT induces less orbital overlap and the red-shifted emission. Since f has a proportional relationship with the square of μ ($f \sim \mu^2$), and $\mu = \iint \phi_L(1)\phi_H(2) r_{12} \phi_L(2)\phi_H(1) d\tau_1 d\tau_2$, thus μ and f can be determined by the orbital overlap and the transition distance. To quantify the overlap between HONTO and LUNTO, we calculated their norm integral S in the Multiwfn program [22]. It can be seen that the S values of DCBP and DCPP are relatively small (~0.44) compared to those of DCFP and DCAP (~0.70), which rationalizes the small μ and f of DCBP and DCPP. To figure out the reason why μ and f of DCAP are also small, we analyzed the orientation of μ and plotted the vectors in Fig. 2b. It is found that the y-components along the short-axes of the molecules are main contributions of μ. The conjoined phenyls in DCAP shortens the transition distance $|r_{12}|$, thus leading to small values of μ and f though the overlap is still large.

3.2. Excited-state decay rate constants

Calculated room-temperature k_r and k_{ic} were illustrated in Fig. 3. According to the k_r formula in Eq. (1), $k_r \sim f\Delta E_{vert}^2$. Therefore, the k_r value of DCFP is largest due to the great f and ΔE_{vert} (Table 2). In comparison with DCFP, the k_r values of the other three "locked" systems are reduced ca. 6–12 fold because of the reduced f and minor- or red-shifted ΔE_{vert}. The k_{ic} values of DCFP and DCBP are both in 10 orders of magnitude, whereas those of DCAP and DCPP are slowed down by ca.

Table 1
Selected dihedral angles (in deg) of DCFP, DCBP, DCAP and DCPP at the S_0/S_1 minimum in solution. Δ represents the structural difference between the optimized S_0 and S_1 states.

	DCFP			DCBP			DCAP			DCPP		
	S_0	S_1	Δ	S_0	S_1	Δ	S_0	S_1	Δ	S_0	S_1	Δ
1	−38.67	−24.03	14.64	12.30	16.31	4.01	0.00	0.00	0.00	−0.08	−0.07	0.01
2	−38.67	−24.03	14.64	−12.30	−16.31	4.01	0.00	0.00	0.00	−0.09	−0.08	0.01

4 orders of magnitude. The k_{ic} sequence can be readily understood in view of the change character in the PES. The steep degree of the PES increases with both the molecular rigidity and conjugation, in the order of DCFP < DCBP < DCAP < DCPP. The rigidity increases in the order of DCFP < DCBP < DCAP ≈ DCPP, which is manifested by the twisting motions of the phenyls (Table 1). The conjugation follows the order of DCFP < DCBP < DCAP < DCPP, which refers to the delocalized π-electron density on the whole molecular backbone. The largest distinction among these systems is that there are two rotational phenyls in DCFP, a constructed four-membered ring in DCBP, a built five-membered ring in DCAP and a newly-formed six-membered ring in DCPP. The overlap between the vibrational states of the S_0 and S_1 states depicts the magnitude of k_{ic}. The steeper the PES, the lower vibrational quanta numbers are involved [23]. Thus, the less effective overlap slows down the internal conversion process.

Either increase k_r or decrease k_{ic} could achieve high emission efficiency since $\Phi_F \approx k_r/(k_r + k_{ic})$. As a result, DCFP and DCBP are calculated to be non-luminescent ($\Phi_f < 0.1\%$) owing to their large k_{ic} values with 10 orders of magnitude. DCPP becomes brightest ($\Phi_f = 76.7\%$) due to its slowest k_{ic} and moderate k_r. The emission of DCAP is weaker ($\Phi_f = 61.0\%$) than DCPP because its k_{ic} value is increased by approximately fourfold, overwhelming the k_r value that is merely increased about twofold. Thus, Φ_f increases in the order of DCFP ≈ DCBP ≪ DCAP < DCPP, in generally consistent with the decrease order of the k_{ic} value. To experimentally verify the above calculated luminescence order of these pyrazine derivatives, we synthesized DCAP and DCPP (Fig. S2-S6). Note the synthesis of DCBP is difficult due to its non-planar conformation and formation of the four-membered ring, but it may exist in the future with the rapid development of the synthetic chemistry [24]. Their Φ_f values were measured for a comparison with the "free" DCFP. Strikingly, the experimental measurements well reproduce the theoretical calculations, in that Φ_f ascends in the order of DCFP (0.015%) ≪ DCAP (4.8%) < DCPP (18.4%). DCFP is non-emissive but both DCAP and DCPP are emissive, as determined from both the calculated and experimental results. Although the calculated Φ_f values are all overestimated, qualitative conclusion can be drawn based on the consistent ascending luminescence order with the experiment. To fully address this issue, an explicit solvent model with a dynamic sampling deserves future investigation [25].

To further find out the critical physical factors affecting the k_{ic} order, we plotted the log (k_{ic}) as a function of the energy gap ΔE (Fig. 4). When ΔE equals to the adiabatic excitation energy ΔE_{ad}, the corresponding value is k_{ic}. According to the k_{ic} formula in Eq. (2), k_{ic} is mainly determined by the total relaxation energy λ, Duschinsky rotation effect (DRE), non-adiabatic electronic coupling (NACME) and ΔE_{ad} [26,27]. The log (k_{ic}) parabola becomes broader with the increase of λ and DRE, enlarging the magnitude of k_{ic}. NACME promotes k_{ic} since it is the pre-factor related to R_{kl}. Small ΔE_{ad} favors large k_{ic} as log (k_{ic}) decreases nearly linearly with ΔE, namely, the energy gap law, when ΔE is large enough. The breadth of the parabola decreases in the order of DCFP>DCBP>DCAP>DCPP, in accord with the descending k_{ic} values. The NACMEs of these systems are quite similar considering the integration of all distributions (Fig. S7). ΔE_{ad} ascends in the order of DCBP < DCPP < DCFP ≈ DCAP, implying partial contradictory effect. Therefore, λ and DRE are two important factors governing the k_{ic} sequence.

3.3. Multimode coupled vibrational relaxations

The relaxation energy λ demonstrates the vibrations' ability to accept the electronic energy of the excited state. Under the harmonic oscillator approximation, λ_j of the j-th normal mode can be defined as $\lambda_j = \hbar S_j \omega_j = \frac{1}{2} D_j^2 \omega_j^2$. S_j is the Huang-Rhys factor and D_j is the mode displacement. λ_j versus ω_j is shown in Fig. 5, with also the aggregation of all modes. It can be seen that the total λ decreases in the order of DCBP

Table 2
Calculated adiabatic excitation energies ΔE_{ad} and vertical emission energies ΔE_{vert} for $S_1 \rightarrow S_0$, as well as the available experimental (exp.) emission peak values (in eV and nm), electric transition dipole moments μ (in Debye), oscillator strength f, HONTO→LUNTO components, overlap integral S of norm of HONTO and LUNTO for DCFP, DCBP, DCAP and DCPP in solution.

	ΔE_{ad}	ΔE_{vert}	exp.	μ	f	HONTO→LUNTO	S
DCFP	3.01 (412)	2.68 (463)	2.93 (423)[a]	4.30	0.19	100.0%	0.7006
DCBP	2.30 (539)	1.94 (638)	N. A.	1.92	0.03	99.6%	0.4439
DCAP	3.06 (405)	2.73 (453)	2.75 (451)[b]	1.71	0.03	99.8%	0.6755
DCPP	2.81 (441)	2.53 (491)	2.55 (487)[b]	1.48	0.02	99.5%	0.4350

[a] Measured in THF, Ref. [8].
[b] Measured in THF, Fig. S1.

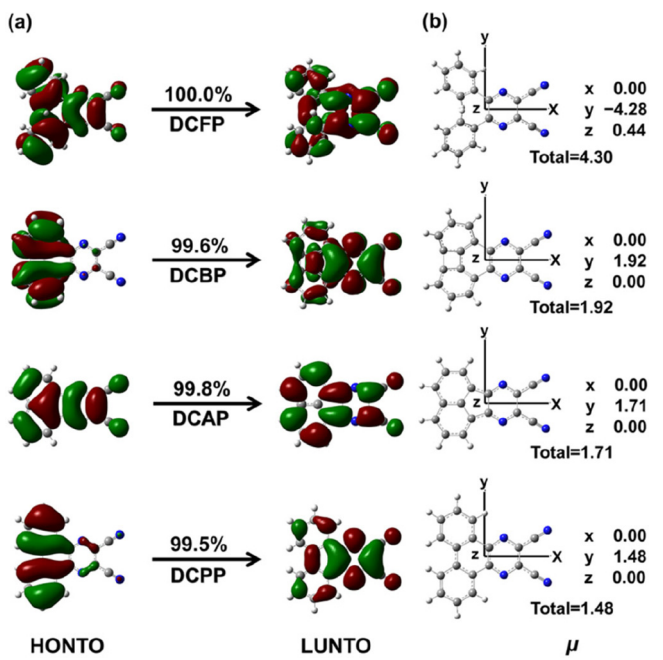

Fig. 2. Transition character and proportion (a), as well as the transition dipole moments μ (in Debye) (b) for the S_1 states of DCFP, DCBP, DCAP and DCPP at their S_1-optimized geometries in solution.

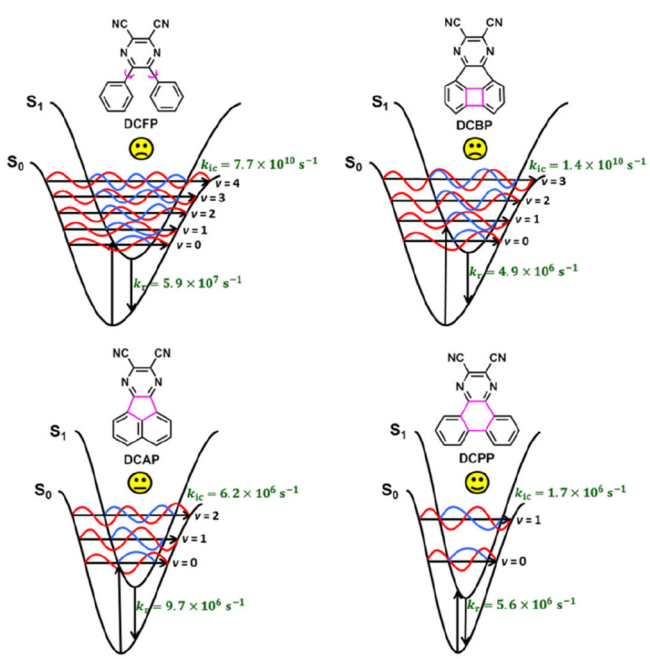

Fig. 3. Sketch of the PESs for DCFP, DCBP, DCAP and DCPP in solution.

> DCAP > DCFP > DCPP, tending to narrow the log (k_{ic}) parabola and reduce the k_{ic} in that order.

λ also reflects the geometric relaxations during the excited-state decay process, and can be projected onto the internal coordinates [28]. Contributions from bond length, bond angle and dihedral angle are listed in Table 3. Detailed internal coordinate representations with large relaxation energies are shown in Fig. S8 and listed in Table S2.

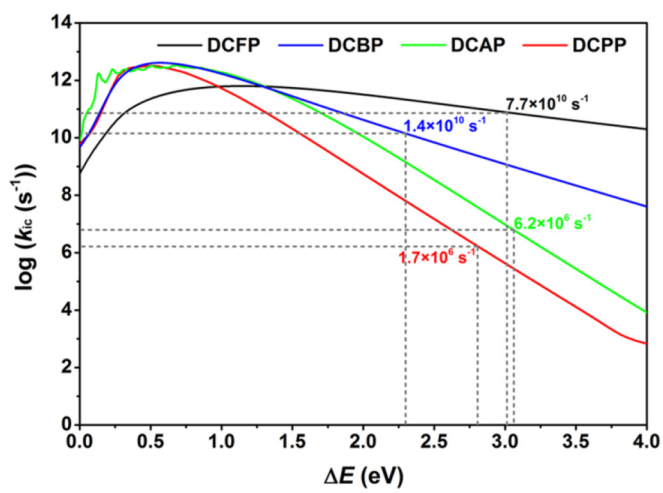

Fig. 4. Calculated logarithm of the non-radiative decay rate log (k_{ic}) versus the energy gap ΔE. The vertical dash line indicates the position of the adiabatic energy gap ΔE_{ad}.

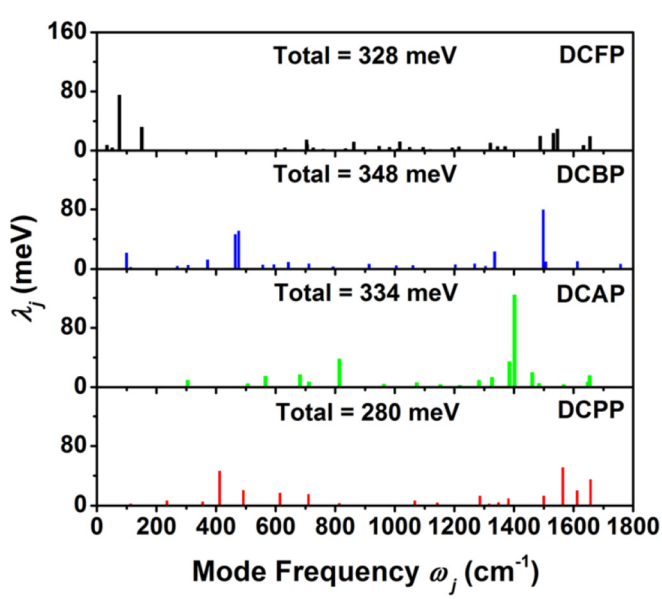

Fig. 5. Relaxation energy λ_j of each normal mode for DCFP, DCBP, DCAP and DCPP in solution.

Table 3
Relaxation energy (meV) from bond length (λ_{bond}), bond angle (λ_{angle}), dihedral angle ($\lambda_{dihedral}$) and the total for DCFP, DCBP, DCAP and DCPP in solution.

	λ_{bond}	λ_{angle}	$\lambda_{dihedral}$	Total
DCFP	177	39	112	328
DCBP	240	74	34	348
DCAP	305	29	0	334
DCPP	207	72	1	280

We found that $\lambda_{dihedral}$ of DCFP is greatest with the value of 112 meV due to the twisting motion of two phenyls. Although the two covalent bonds in DCBP tether the two phenyls to a considerable extent and $\lambda_{dihedral}$ is decreased to 34 meV, the strain of the four-membered ring increases λ_{bond} by 63 meV. At the same time, the "bi-locked" manner introduces more bond angles and increases λ_{angle} by 35 meV. Instead, the total λ of DCBP overwhelms DCFP. Combination of the two phenyls in DCAP thoroughly locks the two phenyls and $\lambda_{dihedral}$ turns into zero. Meanwhile, the "conjoined" architecture produces less bond angles and leads λ_{angle} to the smallest value of 29 meV. However, the strain of the five-membered ring enlarges λ_{bond} to 305 meV, resulting in the total λ of DCAP still a bit larger than DCFP but less than DCBP. The one covalent bond in DCPP fastens the two phenyls and $\lambda_{dihedral}$ is almost null. The "single-locked" way builds the stable six-membered ring and λ_{bond} exhibits a slight increment of 30 meV. Though λ_{angle} is also increased by 33 meV owing to some newly-formed bond angles via linkage, the total λ of DCPP is lower than DCFP and becomes the smallest.

The Huang-Rhys factor S_j characterizes the electron-vibration coupling strength with the modification of the vibrational quanta in the excited-state relaxation process, and S_j versus ω_j is shown in Fig. 6. Notably, the contributions of the low-frequency (<200 cm^{-1}) modes are quite outstanding for DCFP. These modes are mainly assigned to the out-of-plane twisting motions of the phenyl rings and easily dissipate the excited-state electronic energy through mode-mixing, i.e., DRE [9].

DRE measures the coupling among multiple vibrational modes and occurs most remarkably for low-frequency modes with many vibrational states close in energy [16,29]. The serious DRE can spread out the Franck-Condon overlap and largely accelerate k_{ic}. In order to measure the mode-mixing degree, the DRM contour maps for the lowest ten normal modes (not >300 cm^{-1}) are presented. As shown in Fig. 7, the non-diagonal elements are more and large for DCFP but almost null for the others. This indicates that the DRE is severe for DCFP but tiny for the others, leading to its log (k_{ic}) parabola surpass the others and become the broadest. Finally, k_{ic} is reduced in the order of DCFP > DCBP > DCAP > DCPP considering the coupling within and among the vibrational modes.

4. Conclusions

To summarize, we have investigated the excited-state properties of "free" and "locked" pyrazine derivatives in solution using the PCM coupled TVCF approach. It is found that the non-planar DCFP and DCBP are non-emissive and planar DCAP and DCPP are emissive. Compared to the "free" DCFP, k_r values of the other "locked" systems are slightly reduced due to the occurrence of CT or decrement of the transition distance. Through analyses of the non-radiative vibrational relaxation channels, the collective effects of the total relaxation energy λ and DRE result in the decreased k_{ic} order of DCFP > DCBP > DCAP > DCPP. DCFP is non-emissive due to the serious DRE caused by the "free" motion of the phenyls. DCBP is nonluminous because the "bi-locked" manner introduces drastic relaxations through the constructed four-membered ring, leading the total λ to be the largest. DCAP is emissive but not the brightest since the "conjoined" architecture enhances great relaxations via the built five-membered ring, resulting in a moderate λ. The Φ_f value of DCPP is the highest as the "single-locked" way newly forms the stable six-membered ring, giving rise to the smallest λ. Our study suggests that the optical emission properties of the pyrazine derivatives can be tuned by modification of the linkage,

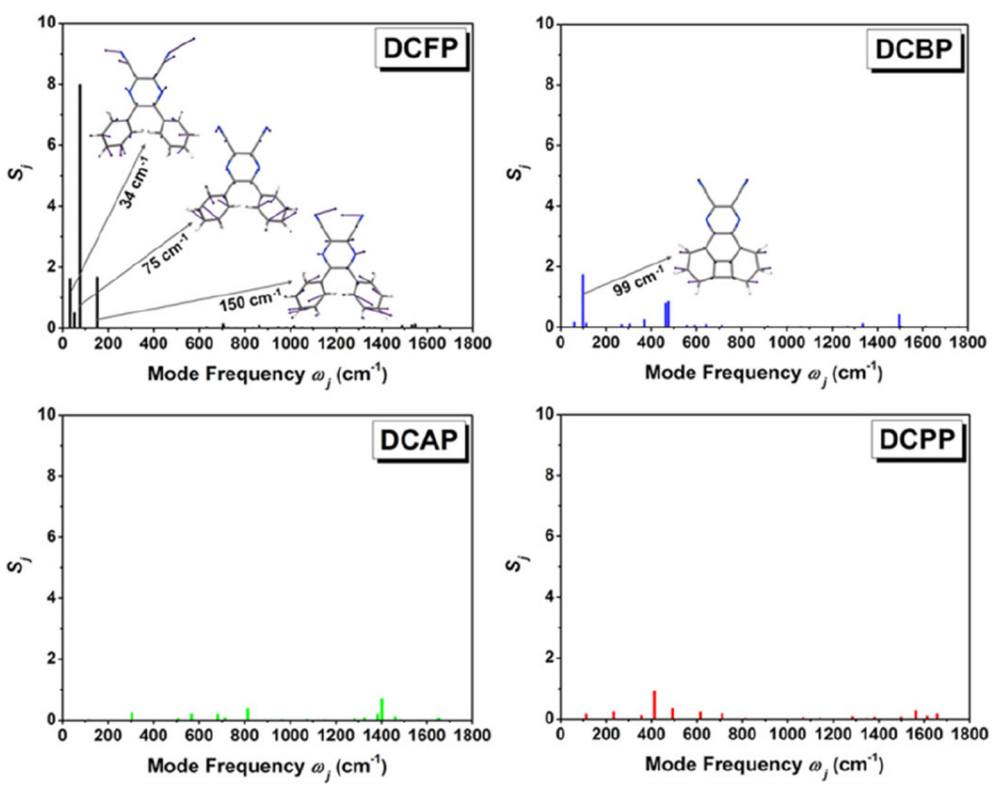

Fig. 6. Huang-Rhys factor S_j of each normal mode for DCFP, DCBP, DCAP and DCPP in solution.

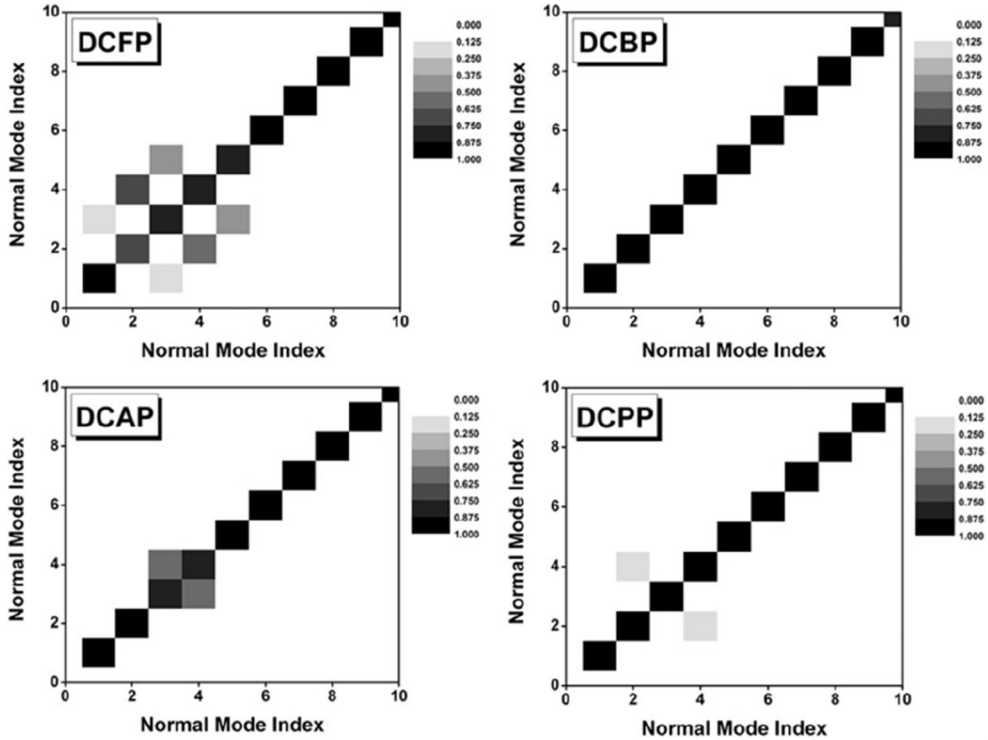

Fig. 7. DRM contour map of the lowest ten normal modes for DCFP, DCBP, DCAP and DCPP in solution.

which is beneficial for the molecular design of efficient organic luminescent materials. Agreement between theoretical calculations and experimental results validates our predicted luminescence order in these pyrazine derivatives, and further supports the restriction of intramolecular motion (RIM) [30] cause for the AIE phenomena.

Finally, we should mention that the methodology we used to study the excited-state properties here are based on a displaced and distorted harmonic oscillator model. Quantitative prediction of the emission quantum efficiency in organic light-emitting materials still consists of challenges [31,32].

Declaration of Competing Interest

There are no conflicts to declare.

Acknowledgement

This work is supported by the National Natural Science Foundation of China (Grant Nos. 21703122, 51673118, 21576159, 21403133, 21403130) and the Natural Science Foundation of Shandong Province (Grant Nos. ZR2017BB034, ZR2019BB067, ZR2014BQ028). Great thanks are expressed to Prof. Qian Peng, Dr. Jianzhong Fan, Dr. Yujun Xie and Guozheng Zhu for their helpful suggestions in our work.

Appendix A. Supplementary data

Supplementary data to this article can be found online at https://doi.org/10.1016/j.saa.2019.117296.

References

[1] Y. Yuan, Y. Hu, Y.-X. Zhang, J.-D. Lin, Y.-K. Wang, Z.-Q. Jiang, L.-S. Liao, S.-T. Lee, Over 10% EQE near-infrared electroluminescence based on a thermally activated delayed fluorescence emitter, Adv. Funct. Mater. 27 (2017) 1700986.

[2] L. Pan, Y. Cai, H. Wu, F. Zhou, A. Qin, Z. Wang, B.Z. Tang, Tetraphenylpyrazine-based luminogens with full-colour emission, Mater. Chem. Front. 2 (2018) 1310–1316.

[3] H.-T. Feng, X. Zheng, X. Gu, M. Chen, J.W.Y. Lam, X. Huang, B.Z. Tang, White-light emission of a binary light-harvesting platform based on an amphiphilic organic cage, Chem. Mater. 30 (2018) 1285–1290.

[4] Z. Qin, Y. Wang, X. Lu, Y. Chen, J. Peng, G. Zhou, Multistimuli-responsive luminescence switching of pyrazine derivative based donor–acceptor–donor luminophores, Chem. Asian J. 11 (2016) 285–293.

[5] J.D. Luo, Z.L. Xie, J.W.Y. Lam, L. Cheng, H.Y. Chen, C.F. Qiu, H.S. Kwok, X.W. Zhan, Y.Q. Liu, D.B. Zhu, B.Z. Tang, Aggregation-induced emission of 1-methyl-1,2,3,4,5-pentaphenylsilole, Chem. Commun. (2001) 1740–1741.

[6] M. Chen, L. Li, H. Nie, J. Tong, L. Yan, B. Xu, J.Z. Sun, W. Tian, Z. Zhao, A. Qin, B.Z. Tang, Tetraphenylpyrazine-based AIEgens: facile preparation and tunable light emission, Chem. Sci. 6 (2015) 1932–1937.

[7] M. Chen, H. Nie, B. Song, L. Li, J.Z. Sun, A. Qin, B.Z. Tang, Triphenylamine-functionalized tetraphenylpyrazine: facile preparation and multifaceted functionalities, J. Mater. Chem. C 4 (2016) 2901–2908.

[8] A.J. Qin, J.W.Y. Lam, F. Mahtab, C.K.W. Jim, L. Tang, J.Z. Sun, H.H.Y. Sung, I.D. Williams, B.Z. Tang, Pyrazine luminogens with "free" and "locked" phenyl rings: understanding of restriction of intramolecular rotation as a cause for aggregation-induced emission, Appl. Phys. Lett. 94 (2009), 253308.

[9] C.M. Deng, Y.L. Niu, Q. Peng, A.J. Qin, Z.G. Shuai, B.Z. Tang, Theoretical study of radiative and non-radiative decay processes in pyrazine derivatives, J. Chem. Phys. 135 (2011), 014304.

[10] Q.Y. Wu, C.M. Deng, Q. Peng, Y.L. Niu, Z.G. Shuai, Quantum chemical insights into the aggregation induced emission phenomena: a QM/MM study for pyrazine derivatives, J. Comput. Chem. 33 (2012) 1862–1869.

[11] C. Lee, W.T. Yang, R.G. Parr, Development of the Colle-Salvetti correlation-energy formula into a functional of the electron density, Phys. Rev. B 37 (1988) 785–789.

[12] A.D. Becke, Density-functional thermochemistry. III. The role of exact exchange, J. Chem. Phys. 98 (1993) 5648–5652.

[13] M.J. Frisch, G.W. Trucks, H.B. Schlegel, G.E. Scuseria, M.A. Robb, J.R. Cheeseman, G. Scalmani, V. Barone, G.A. Petersson, H. Nakatsuji, X. Li, M. Caricato, A.V. Marenich, J. Bloino, B.G. Janesko, R. Gomperts, B. Mennucci, H.P. Hratchian, J.V. Ortiz, A.F. Izmaylov, J.L. Sonnenberg, D. Williams-Young, F. Ding, F. Lipparini, F. Egidi, J. Goings, B. Peng, A. Petrone, T. Henderson, D. Ranasinghe, V.G. Zakrzewski, J. Gao, N. Rega, G. Zheng, W. Liang, M. Hada, M. Ehara, K. Toyota, R. Fukuda, J. Hasegawa, M. Ishida, T. Nakajima, Y. Honda, O. Kitao, H. Nakai, T. Vreven, K. Throssell, J.A. Montgomery Jr., J.E. Peralta, F. Ogliaro, M.J. Bearpark, J.J. Heyd, E.N. Brothers, K.N. Kudin, V.N. Staroverov, T.A. Keith, R. Kobayashi, J. Normand, K. Raghavachari, A.P. Rendell, J.C. Burant, S.S. Iyengar, J. Tomasi, M. Cossi, J.M. Millam, M. Klene, C. Adamo, R. Cammi, J.W. Ochterski, R.L. Martin, K. Morokuma, O. Farkas, J.B. Foresman, D.J. Fox, Gaussian16 Revision B.01, Gaussian, Inc., Wallingford, CT, 2016.

[14] J. Tomasi, B. Mennucci, R. Cammi, Quantum mechanical continuum solvation models, Chem. Rev. 105 (2005) 2999–3094.

[15] Z.D. Li, Y.L. Xiao, W.J. Liu, On the spin separation of algebraic two-component relativistic hamiltonians, J. Chem. Phys. 137 (2012), 154114.

[16] Q. Peng, Y.P. Yi, Z.G. Shuai, J.S. Shao, Toward quantitative prediction of molecular fluorescence quantum efficiency: role of Duschinsky rotation, J. Am. Chem. Soc. 129 (2007) 9333–9339.
[17] Y.L. Niu, Q. Peng, C.M. Deng, X. Gao, Z.G. Shuai, Theory of excited state decays and optical spectra: application to polyatomic molecules, J. Phys. Chem. A 114 (2010) 7817–7831.
[18] S.H. Lin, Rate of interconversion of electronic and vibrational energy, J. Chem. Phys. 44 (1966) 3759–3767.
[19] Y.L. Niu, W.Q. Li, Q. Peng, H. Geng, Y.P. Yi, L.J. Wang, G.J. Nan, D. Wang, Z.G. Shuai, MOlecular MAterials Property Prediction Package (MOMAP) 1.0: a software package for predicting the luminescent properties and mobility of organic functional materials, Mol. Phys. 116 (2018) 1078–1090.
[20] U. Ghosh, D. Ganessunker, V.J. Sattigeri, K.E. Carlson, D.J. Mortensen, B.S. Katzenellenbogen, J.A. Katzenellenbogen, Estrogenic diazenes: heterocyclic nonsteroidal estrogens of unusual structure with selectivity for estrogen receptor subtypes, Bioorg. Med. Chem. 11 (2003) 629–657.
[21] R.L. Martin, Natural transition orbitals, J. Chem. Phys. 118 (2003) 4775–4777.
[22] T. Lu, F. Chen, Multiwfn: a multifunctional wavefunction analyzer, J. Comput. Chem. 33 (2012) 580–592.
[23] F. Bu, R.H. Duan, Y.J. Xie, Y.P. Yi, Q. Peng, R.R. Hu, A.J. Qin, Z.J. Zhao, B.Z. Tang, Unusual aggregation-induced emission of a coumarin derivative as a result of the restriction of an intramolecular twisting motion, Angew. Chem. Int. Ed. 54 (2015) 14492–14497.
[24] K.R. Campos, P.J. Coleman, J.C. Alvarez, S.D. Dreher, R.M. Garbaccio, N.K. Terrett, R.D. Tillyer, M.D. Truppo, E.R. Parmee, The importance of synthetic chemistry in the pharmaceutical industry, Science 363 (2019) 244.
[25] N. De Mitri, S. Monti, G. Prampolini, V. Barone, Absorption and emission spectra of a flexible dye in solution: a computational time-dependent approach, J. Chem. Theory Comput. 9 (2013) 4507–4516.
[26] Z.G. Shuai, Q. Peng, Excited states structure and processes: understanding organic light-emitting diodes at the molecular level, Phys. Rep. 537 (2014) 123–156.
[27] T. Zhang, W. Shi, D. Wang, S. Zhuo, Q. Peng, Z.G. Shuai, Pressure-induced emission enhancement in hexaphenylsilole: a computational study, J. Mater. Chem. C 7 (2019) 1388–1398.
[28] J.R. Reimers, A practical method for the use of curvilinear coordinates in calculations of normal-mode-projected displacements and Duschinsky rotation matrices for large molecules, J. Chem. Phys. 115 (2001) 9103–9109.
[29] T. Zhang, Q. Peng, C.Y. Quan, H. Nie, Y.L. Niu, Y.J. Xie, Z.J. Zhao, B.Z. Tang, Z.G. Shuai, Using the isotope effect to probe an aggregation induced emission mechanism: theoretical prediction and experimental validation, Chem. Sci. 7 (2016) 5573–5580.
[30] M. Zhang, L. Zhao, R. Zhao, Z. Li, Y. Liu, Y. Duan, T. Han, A mechanochromic luminescent material with aggregation-induced emission: application for pressure sensing and mapping, Spectrochim. Acta A 220 (2019), 117125.
[31] Z.G. Shuai, Q. Peng, Organic light-emitting diodes: theoretical understanding of highly efficient materials and development of computational methodology, Natl. Sci. Rev. 4 (2017) 224–239.
[32] J. Fan, Y. Zhang, K. Zhang, J. Liu, G. Jiang, F. Li, L. Lin, C.-K. Wang, Theoretical arrangement of thermally activated delayed fluorescence as host for fluorescent emitter with blue to red emission, Spectrochim. Acta A 219 (2019) 44–52.